

# Robust Methods for Detecting Spontaneous Activations in fMRI Data



Francesca Gasperoni and Alessandra Luati

**Abstract** Functional magnetic resonance imaging (fMRI) is a technique for measuring brain activity. The outcomes of fMRI measurements are complex data that can be interpreted as multivariate time series, recorded at different brain locations, usually across subjects. The literature has been mainly concerned with task-based fMRI analysis, which focuses on the response to controlled exogenous stimuli. Nevertheless, resting state fMRI (RfMRI) analysis, dealing with spontaneous brain activity, is considered the key to understand the neuronal organisation of the brain. The aim of this paper is to identify spontaneous neural activations and to estimate the brain response function in RfMRI data, called Hemodynamic Response Function (HRF). To this purpose, we apply an existing method based on a normality assumption for the data generating process and we consider a novel, more general method, based on robust filtering. Finally, we compare the neural activations and HRF estimates for two specific patients.

**Keywords** BOLD signal · Heavy tails · HRF estimation · Resting state  
Robust filtering · Spatial dependence

## 1 Introduction

Functional magnetic resonance imaging (fMRI) is a non invasive technique for collecting data on brain activity, with a good resolution in terms of space and time. Essentially, fMRI measures the increase in the oxygenation level at some specific

---

F. Gasperoni (✉)

MOX, Department of Mathematics, Politecnico di Milano, Milan, Italy  
e-mail: [francesca.gasperoni@polimi.it](mailto:francesca.gasperoni@polimi.it)

A. Luati

Department of Statistics, University of Bologna, Bologna, Italy  
e-mail: [alessandra.luati@unibo.it](mailto:alessandra.luati@unibo.it)

© Springer Nature Switzerland AG 2018

A. Canale et al. (eds.), *Studies in Neural Data Science*, Springer Proceedings  
in Mathematics & Statistics 257, [https://doi.org/10.1007/978-3-030-00039-4\\_6](https://doi.org/10.1007/978-3-030-00039-4_6)

brain region, as long as an increase in blood flow occurs, due to some brain activity. The latent signal in the observed fMRI data is referred to as the blood oxygenation level dependent (BOLD) signal.

A large stream of the literature has dealt with the analysis of task based experiments, where the BOLD is measured in response to some stimulus or event. On the other hand, only in recent years the interest has been concentrating toward resting state fMRI (RfMRI), as the key to understand the neuronal organisation of the brain, through the investigation of the spatial and temporal structure of spontaneous neural activity. The earliest work that focused on RfMRI was the one of Biswal et al. [2], where it is shown that the same brain regions that were active and correlated during finger tapping were also correlated with the spontaneous BOLD fluctuations in the absence of any stimulus. Since then, growing attention has been devoted to RfMRI data analysis. In the review paper by Biswal [3], resting state fMRI is described as the candidate approach capable of addressing the core challenge in neuroimage, i.e., the development of common paradigms for interrogating the functional systems in the brain, without the constraint of a priori hypotheses.

When analysing fMRI series, major inferential issues arise, due to the complexity of the data. As a matter of fact, fMRI are recorded as high frequency time series, observed at different brain region of interests (ROI) or, on a finer scale, at different voxels, across individuals. Hence, besides the intrinsic dynamic nature of fMRI, the researcher has to take into account aspects like curse of dimensionality at the voxel level, presence of explanatory variables depending on the design of the experiment, spatial correlation, which is of interest for connectivity analysis, as well as multivariate aspects related to multisubject or group analysis.

Despite specifically depending on the aim of the analysis, the most common approach followed to analyse fMRI data consists in a sequence of analytical steps that eventually result in a general linear model accounting for time and space correlation. The basic assumption for the first step, that is a univariate time series analysis, consists in a simple decomposition of pre-processed fMRI data into an unobserved signal plus noise. The underlying hypothesis on the two latent variables are related to the evolution of the components in the time and with the dependence on some explanatory variables. Once the dynamic characteristics of the series are acknowledged, their interrelation across ROIs and subjects becomes the main object of the analysis, so that methods ranging from spatial modelling to large covariance matrix estimation are required.

Most of the models used for the time series analysis of fMRI assume a stationary Gaussian distribution for the noise term. However, the stationarity hypothesis seems to be not justifiable and the assumptions on the dynamics in fMRI are still controversial. Indeed, there is still a considerable debate on the dynamic properties of fMRI and  $AR(p)$  errors have been considered, see e.g. [23, 27], as well as fractional noise error processes [5], and recently change point methods [1] as an alternative to stationarity. Moreover, Lund et al. in [24] concluded that no commonly accepted model for noise in fMRI exists and that regressors may whiten the noise as well as high pass filters. In resting state studies, the dynamics of the noise component are even more relevant than in task based experiments, as recognised in [12], since, ideally,

no exogenous stimulus affects the underlying signal and the noise dynamics reflect the human brain resting activity.

In this paper, we aim at specifying a model with more general assumptions on the noise term, which is allowed to be non Gaussian, and on the signal, which is a possibly non stationary dynamic process that may depend on estimated hemodynamic response functions specifically designed for spontaneous neural activity.

The first contribution of our analysis is indeed the estimation of the hemodynamic response function, and consequently, of the potential explanatory variables for the signal of RfMRI data. In the case of resting state experiments, the challenge lies in the specification of an impulse response function that accounts for spontaneous neural activity in the absence of controlled stimulus for each ROI. Considering a general regression model with Gaussian stationary autocorrelated errors, Wu et al. in [29] designed a strategy for HRF reconstruction based on the identification of spontaneous activations as extreme values from a Gaussian distribution. As pointed out in [28], the problem of detecting spontaneous activations has much in common with outlier detection. Our idea is then to identify spontaneous activations as outliers of a Normal distribution or as extreme values of a heavy tailed distribution. Specifically, we assume a Student- $t$  distribution for the noise term and identify spontaneous activations as extreme values of residuals obtained from a robust procedure for signal extraction, as in [18]. Modeling the data under the assumption of a heavy tail distribution for the noise affecting the BOLD signal is the second contribution of the paper.

We shall estimate and compare the HRF obtained from the two methods and illustrate the results on two patients and four ROIs. Spatial dependence will be explored through the investigation of a proper similarity index for binary data. In particular, we compute and plot the similarity matrices related to the estimated spontaneous events across ROIs. Thanks to this approach, we are able to detect and study groups of ROIs with the highest similarity.

The paper is organised as follows. Section 2 describes the methods used for identifying the spontaneous activations and estimating the HRF. Section 3 illustrates the results of the analysis obtained in four specific ROIs of two patients. Section 4 concludes the paper with some directions for further research.

## 1.1 Dataset Description

The multimodal imaging dataset that we are considering comes from a pilot study of the Enhanced Nathan Kline Institute-Rockland Sample project. This project aims at providing a large cross-sectional sample of publicly shared multimodal neuroimaging data and psychological information to support and motivate researchers in the relevant scientific goal of understanding the mechanisms underlying the complex brain system. A detailed description of the project, scopes, and technical aspects can be found at [http://fcon\\_1000.projects.nitrc.org/indi/enhanced/](http://fcon_1000.projects.nitrc.org/indi/enhanced/). The pilot NK11

study comprises multimodal imaging data and subject-specific covariates for  $n = 24$  subjects. Detailed information can be found at [http://fcon\\_1000.projects.nitrc.org/indi/CoRR/html/nki\\_1.html](http://fcon_1000.projects.nitrc.org/indi/CoRR/html/nki_1.html). An appealing aspect of this pilot study, compared to the whole dataset, is that for a wide set of subjects scan-rescan imaging data are available, thereby allowing validation and inference also on subject-specific variability in brain functions and structures.

For each subject several information are collected, both personal covariates (i.e., anxiety diagnosis, age, gender, handedness) and BOLD signals, which are recorded for all 70 ROIs according to Desikan atlas. For such  $V = 70$  regions we have additional information on 3-D spatial locations, hemisphere and lobe membership. One region, in the left and right hemisphere, is marked as unknown, and typical analyses consider only the 68 regions characterizing the Desikan atlas.

We have the following datasets:

- (1) **Structural networks**,  $70 \times 70 \times 24 \times 2$ , comprising the  $70 \times 70$  structural connectivity networks collected for the 24 subjects in each of the 2 scan-rescan imaging sessions.

Focusing on subject  $i$  and on scan  $k$ , where  $i = 1, \dots, 24$  and  $k = 1, 2$ , we have a  $70 \times 70$  symmetric adjacency matrix measuring the total number of white matter fibers connecting each pair of brain regions.

- (2) **Dynamic functional activity**,  $70 \times 404 \times 24 \times 2$ , comprising the  $70 \times 404$  multivariate time-series data collected for each subject in each of the 2 scan-rescan imaging sessions.

This imaging technology monitors brain functional activity at different regions via dynamic changes in blood flow creating a low frequency BOLD signal when the subject is not performing an explicit task during the imaging session. In the present NKI1 study, the subjects are simply asked to stay awake with eyes open. Focusing on subject  $i$  and on scan  $k$ , where  $i = 1, \dots, 24$  and  $k = 1, 2$ , we have  $70 \times 404$  matrix whose rows contain the dynamic activity data of the brain regions, collected at  $T = 404$  equally spaced times (time lag is 1400 ms).

- (3) **Functional networks**,  $70 \times 70 \times 24 \times 2$ , measuring synchronization in activity for each pair of brain regions (obtained through Pearson correlation of the previous dataset fixing the ROI, the subject and the scan).

Our major interest lays on the investigation of differences among subjects, based on the dynamic functional activity of their brains, so we focus on the second dataset.

Moreover, we have ROI-specific information. Not having voxel-specific data leads to small data, which means that we expect not to have computational issues and therefore we shall not need to apply dimension reduction techniques such as principal component analysis (PCA) or independent component analysis (ICA).

## 2 Modelling fMRI Data

The most common approach for analysing fMRI data is based on General Linear Models (GLM), where the observed fMRI is taken as the response variable, while the BOLD signal is modelled through a set of explanatory variables, usually taken as the HRF and its temporal and dispersion derivatives. The latter are the partial derivatives with respect to the two parameters that characterise the canonical HRF distribution: the time to peak and the width of the HRF at half the height (Chap. 14 in [20]). On one hand, the estimate of temporal derivatives allows us to capture small changes in the latency of the response, on the other hand, the estimate of dispersion derivatives allows us to capture differences in the duration of the peak response.

A stationary Gaussian process with non-spherical covariance matrix is assumed for the noise term. This approach is usually named general linear model and it has been studied in literature at individual level [26]. A common choice for the HRF is the double-gamma function, which can be derived through a deconvolution process between a stimulus function and the BOLD signal. The choice of the stimulus function is straightforward when task based experiments are considered (e.g. a step function), but it is not trivial in case of RfMRI.

The main contribution of this paper consists in the estimate of RfMRI hemodynamic response functions at the ROI level, with two different methodologies: on one hand, we take advantage of the blind deconvolution technique proposed in [29]; on the other hand, we consider a more general method, based on robust filtering, developed in [18]. We then compare the performance of the two methods in terms of spontaneous activation detection and analyse the estimated parameters that characterize the HRF.

Both methods are based on a signal plus noise decomposition,

$$y_t = \mu_t + \varepsilon_t$$

where  $y_t$ ,  $t = 1, 2, \dots, T$ , is the observed fMRI data (in fMRI, the term functional refers to time series data),  $\mu_t$  is the unobserved BOLD signal and  $\varepsilon_t$  is a noise term.

In the framework of general linear modelling, where the blind deconvolution technique is developed [29], the signal is explained by a set of (estimated, see Sect. 2.2) HRF and the noise is a first order Gaussian autoregressive process, i.e.  $\mu_t = X_t\beta$  and  $\varepsilon_t = \phi\varepsilon_{t-1} + \eta_t$  where  $\eta_t \stackrel{i.i.d}{\sim} N(0, \sigma^2)$  and  $|\phi| < 1$ .

The alternative model we are considering here assumes that the noise is a Student- $t$  process,  $\varepsilon_t \sim t_\nu(0, \sigma^2)$ , while the signal follows a first order autoregressive model,  $\mu_t = X_t\beta + \phi\mu_{t-1} + \kappa u_{t-1}$ , where  $u_t$  is a martingale difference sequence, i.e.,  $E(u_t|\mathcal{F}_{t-1}) = 0$ ,  $\mathcal{F}_{t-1}$  represents the information set up to time  $t - 1$ , and  $|\phi| \leq 1$ , i.e., the model can account for non stationary components. This model belongs to the class of score driven models, recently introduced in [9] and in [19].

These are nonlinear observation driven models where the dynamic parameters ( $\mu_t$  in our case) are updated by filters that are robust with respect to extreme values. The robustness comes from the properties of the martingale difference sequence  $u_t$  that

drives the dynamics of the time varying parameter. The main feature of score driven models is that  $u_t$  is proportional to the score of the conditional (with respect to  $\mathcal{F}_{t-1}$ ) likelihood of  $\mu_t$ . When the data come from a heavy tail distribution, the score  $u_t$  is less sensitive to extreme values than the score of a Gaussian distribution or than the innovation error  $v_t = X_t - \mu_t$ . We shall further discuss the robustness properties of the model in Sect. 2.2.

The static parameters,  $\nu, \phi, \kappa, \sigma$  in our case, are consistently estimated by maximum likelihood and asymptotic standard errors can be derived [18, 19]. An important property of the proposed specification is that it encompasses the Gaussian case, in that the score of the Student- $t$  converges to that of the Gaussian distribution when the degrees of freedom tend to infinity. In practice, if a score driven model is estimated when the underlying dataset is in fact Gaussian, a very high value for the degrees of freedom is estimated and a Gaussian model is eventually fitted.

## 2.1 The BOLD Signal

The BOLD signal arises from the interplay of blood flow, blood volume, and blood oxygenation in response to changes in neural activity. Under an active state, the local concentration of oxygenated hemoglobin increases, with a corresponding increase in the homogeneity of magnetic susceptibility, which, in turn, results in an increase of MRI signal. The BOLD signal does not increase instantaneously and does not return to baseline immediately after the stimulus ends. Because these changes in blood flow are relatively slow (evolving over several seconds), the BOLD signal is a blurred and delayed representation of the original neural signal. The HRF can be described as the ideal, noiseless response to an infinitesimally brief stimulus. Five characteristics determine the HRF: time from the stimulus until peak (TP, or time-to-peak), height of response (H), the width of the HRF at half the height (FWHM), poststimulus undershoot (PSU) and initial dip (ID), see Fig. 1 reproduced from [25]. Importantly, there is substantial variability in each of these features of the HRF across brain areas and across individuals. For example, in [21], the time until peak varied between 6 and 11 seconds across voxels in a single subject. In [17], a study of the HRF shape revealed that both the time until peak and width of the HRF varied within subjects across different regions of the brain and across subjects, with intersubject variability higher than intrasubject variability. D’Esposito et al. in [10] reviewed a number of studies that compared the BOLD signal in healthy young and old subjects and found, while the shape of the HRF was similar between the groups, elderly had reduced signal-to-noise ratios in the response magnitudes.

The HRF is not observed, i.e., it is not recorded by medical instruments, but it has to be estimated from the observed fMRI series based on some underlying assumptions on its behaviour in time. To this aim, a widely recognized technique in neuroscience is the convolution between a controlled temporal stimulus and an unobservable hemodynamic response, depending on an unknown static parameter. Additively combined with a zero mean noise, the convolution results in an explana-

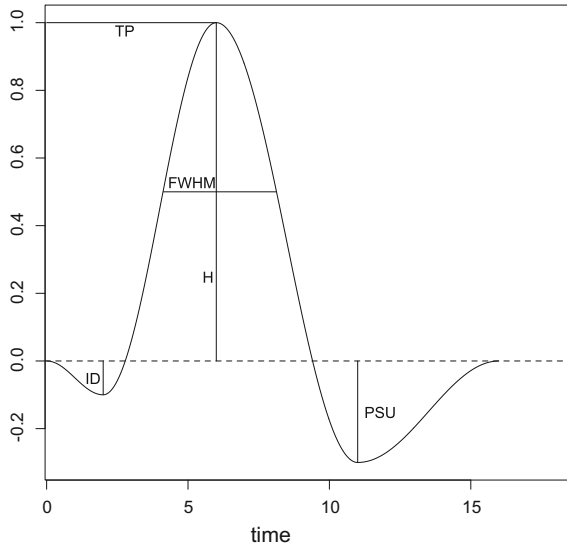


**Fig. 1** Example of a hemodynamic response function (HRF). The abscissa reports the time, in seconds, ranging from 0 (occurrence of the stimulus) to 15 s (following the post-stimulus undershoot, when the level returns to the baseline); the ordinates report the value of hemodynamic response function across time on a standardised scale from 0 to 1. The main characteristics of HRF are highlighted: time from the stimulus until peak (TP), height of response (H), the width of the HRF at half the height (FWHM), poststimulus undershoot (PSU) and initial dip (ID)

tory variable for the observed data, which reflects that neural response and the BOLD signal exhibit linear time invariant (LTI) properties. By applying deconvolution models, Friston et al. in [15] and Lange and Zeger in [22] found out that in general HRF could be described by a gamma function. However, this function is not able to capture the poststimulus undershoot which characterizes the HRF, so later on Friston et al. in [14] and Glover in [16] proposed a combination of two gamma functions, known as double-gamma, for describing the HRF. All these studies are related to task based fMRI, when a deconvolution procedure according to the explicit task design is possible. Methods for estimating the HRF and the role of the HRF in case of RfMRI are far less explored in literature.

A first attempt to estimate the HRF in RfMRI through a blind-deconvolution technique is described in [29]. The latter is illustrated in the next section along with our alternative strategy.

## 2.2 HRF Estimation

In task based experiments, HRF estimation is based on the convolution of some basis function,  $x_{BF}$ , with an activation function which accounts for the stimulus,  $s_t$ , that

is usually represented by a step function or by a series of delta functions, according to the experimental design (e.g., finger-tapping, hot-cold exposure).

In resting state analysis, where no external stimuli are recorded, spontaneous activations, commonly referred to as spontaneous low-frequency fluctuations, as in [12] or spontaneous neural state, as in [29], should be estimated, hence the reference to  $\hat{s}_t$ . In the current analysis,  $\hat{s}_t$  will be a binary time series of zeros and ones with one corresponding to activation and zero to rest. The key idea behind the identification of the time series of spontaneous events is that it can be expressed as a sequence of delta functions that are activated in correspondence of extreme values of a Gaussian or Student- $t$  distribution. The idea is motivated by the fact that time series extreme values can be seen as spontaneous neural activations of the brain.

Once the spontaneous events are detected, and this is the central focus of this work, the estimated HRF is obtained by the estimation procedure shown in [29], for the two models illustrated in the introduction of Sect. 2.

The overall HRF estimation strategy can be summarised as follows:

- (i) estimate the spontaneous activations  $\hat{s}_t$ ;
- (ii) find a preliminary estimate of the design matrix  $X_t$  as the convolution of  $\hat{s}_t$  with a suitable basis function (a canonical double gamma function, in this case)  $x_{BF}$ , as follows,

$$X_t = \hat{s}_t \otimes x_{BF} = \int_{-\infty}^{+\infty} \hat{s}_t \cdot x_{BF}(t - \tau) d\tau;$$

- (iii) plug the preliminary estimate of  $X_t$  as the matrix containing the explanatory variables in the Gaussian or Student- $t$  model, in order to obtain an estimate of the coefficients  $\hat{\beta}$ ;
- (iv) obtain the HRF estimate as  $\hat{h}_t = x_{BF}\hat{\beta}$ .

We now discuss the procedure under the Gaussian linear model and the Student- $t$  non linear model described in the introduction of Sect. 2.

Under the Gaussian model in the formulation proposed in [29], spontaneous activations are estimated by standardising the original data and marking as outliers those points that exceed a certain cut-off, fixed at  $1.65\hat{\sigma}$ , i.e., the 10% of extreme values of each series are considered as spontaneous activations. The preliminary estimate of the design matrix  $X_t$  is then obtained by the convolution of  $\hat{s}_t$  with an HRF basis, chosen as a classical double gamma with its first derivative and dispersion derivative. Then, an estimate of  $\beta$  is obtained (along with that of  $\phi$ ) by the Cochrane-Orcutt procedure. Finally,  $\hat{h}_t = x_{BF}\hat{\beta}$ . Figures 10 and 11 will report examples of estimated HRF on the case study considered in the paper. Note that  $\hat{h}_t$ , the estimated HRF is not  $\hat{\mu}_t$ , the estimated signal  $\hat{\mu}_t = \hat{X}_t\hat{\beta}$  though some circularity affects procedure of BOLD estimation in [29]. The aim, here, is mainly to estimate the HRF rather than the BOLD signal.

Under the Student- $t$  model in the formulation proposed in [18], described in the introduction of Sect. 2, spontaneous activations are estimated by considering as extreme values those values of  $v_t = y_t - \hat{\mu}_t$  which exceed the threshold  $\max\{\hat{\kappa}u_t\}$  if  $\hat{\kappa} > 1$  or  $\max\{u_t\}$  if  $\hat{\kappa} < 1$  where, under the assumptions of the model,  $v_t$ , the



one-step-ahead prediction error, has a Student- $t$  distribution while  $u_t$ , the martingale different sequence proportional to the score of the Student- $t$  that drives the dynamics of the BOLD signal, has a thin tailed distribution. The selection of the threshold is motivated as follows. In practice,  $u_t$  itself is a thresholded version of  $v_t$ , where extremes are cut off by construction, as  $u_t = v_t / (1 + v_t^2 / (\nu\sigma^2))$ . The parameter  $\kappa$  further regulates the thresholding of  $v_t$ , and thus the robustness of  $\hat{\mu}_t$ . A natural choice for the threshold then relates to the case when  $\hat{\kappa} > 1$  versus the case when  $\hat{\kappa} \leq 1$ . We choose to take as extremes those values of  $v_t$  which exceed  $u_t$  by keeping the estimated  $\hat{\kappa}u_t$  when  $\hat{\kappa} > 1$  and  $u_t$  otherwise. The opposite choice would lead to a larger number of outlying observations, i.e., of spontaneous activations. The preliminary estimate of the design matrix  $X_t$  is obtained, as in the Gaussian case, by the convolution of  $\hat{s}_t$  with the HRF basis formed by the double gamma with its first derivative and dispersion derivative. An estimate of  $\beta$  is obtained (along with that of all the static parameters of the model) by maximum likelihood in the case when explanatory variables are included in the model, see [18] Sect. 7. Finally,  $\hat{h}_t = x_{BF}\hat{\beta}$ , see Figs. 10 and 11. The estimated HRF  $\hat{h}_t$  may then be considered as an explanatory variable for the filtered signal,  $\mu_t = \hat{h}_t\gamma + \phi\mu_{t-1} + \kappa u_{t-1}$ . As before, focus here was primarily on HRF estimation, but we aim at further pursuing this analysis in future research.

### 3 Illustrative Examples

We focus on patients 18 and 22 and on ROI 64, 51, 63, 59, for reasons explained below.

Patient 18 is 46 years old, right-handed and healthy while 22 is 42 years old, right-handed and has a diagnosis of depression with a clinical history of alcohol, cannabis and cocaine abuse. Our aim consists in investigating and comparing brain connections in these two subjects.

According to Fox et al. [13], some brain regions have positive correlations, while other brain regions show negative correlations. In particular, there is a positive correlation among frontal eye field (FEF), intraparietal (IPS) and middle temporal region (MT), while there is a negative correlation among medial prefrontal cortex (MPF), posterior cingulate precuneus (PCC) and lateral parietal cortex (LP). In our dataset, we do not have the same atlas representation of the brain, so we have to find the correspondence between our atlas and the one used in [13]. After this procedure, we analyze the following brain regions:

- **Positive correlation:** ROI 64 (rh-frontal superior, for FEF) and ROI 51 (rh-middle temporal, for MT);
- **Negative correlation:** ROI 63 (rh-rostral middle frontal, for MPF) and ROI 59 (rh-posterior cingulate, for PCC).

In our dataset, the lateral parietal cortex cannot be distinguished from the intraparietal sulcus and this is the reason why we focus only on the correlation between two regions of interest.

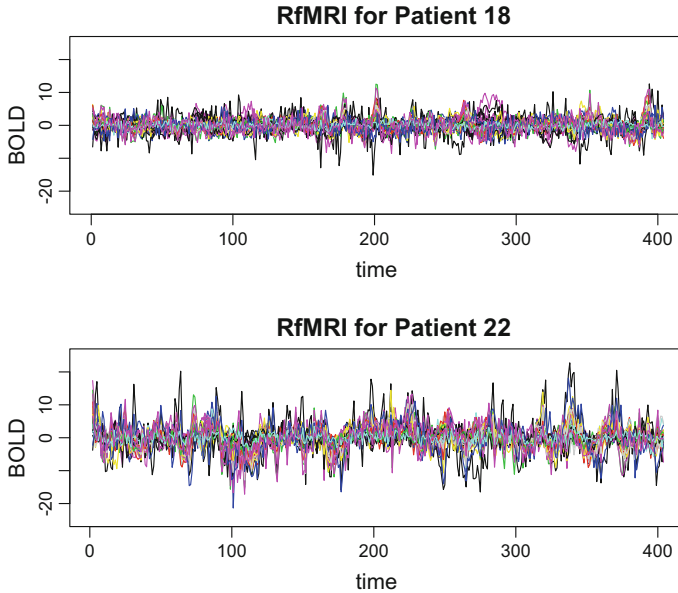


**Fig. 2** Observed RfMRI series at all ROI for subjects 18 and 22

The 70 observed fMRI series for patients 18 and 22, first scan, are represented in Fig. 2. One can immediately notice the difference of range and amplitude of the fluctuations between the two series, being the variability of fMRI of patient 22 larger than that of patient 18.

We proceed to compare the estimated  $\hat{s}_t$  with both methods. Spontaneous events detected in the time series of ROI 64, 51, 63 and 59 for patient 18 are reported in Fig. 3, those detected in the time series of the same ROI for patient 22 are reported in Fig. 4. We remark here that the number of spontaneous activations detected under the hypothesis of a Student- $t$  model for patient 22 drastically drops down if the first extreme observation is removed from the series, compare Figs. 4 and 5. Nevertheless, we illustrate the results of the analysis on the original series including the first observation. The method based on the assumption of a Student- $t$  distribution for the noise is expected to select a smaller number of spontaneous activations than the method based on the Gaussian assumption. However, several series analysed in the dataset turned out to be Gaussian, in which case the two methods give, as expected, similar results.

Despite of the fact that similar peaks are detected (ROI 63 in Fig. 3), we would like to understand whether there are correlations among activations of different brain regions and whether the two methods used for detecting peaks lead to different results. In order to further investigate this idea, we need a concept of distance/similarity for binary vectors. Indeed, standard correlation indices, such as Pearson's correlation index, are not suitable for this case. There are several similarity indices for binary

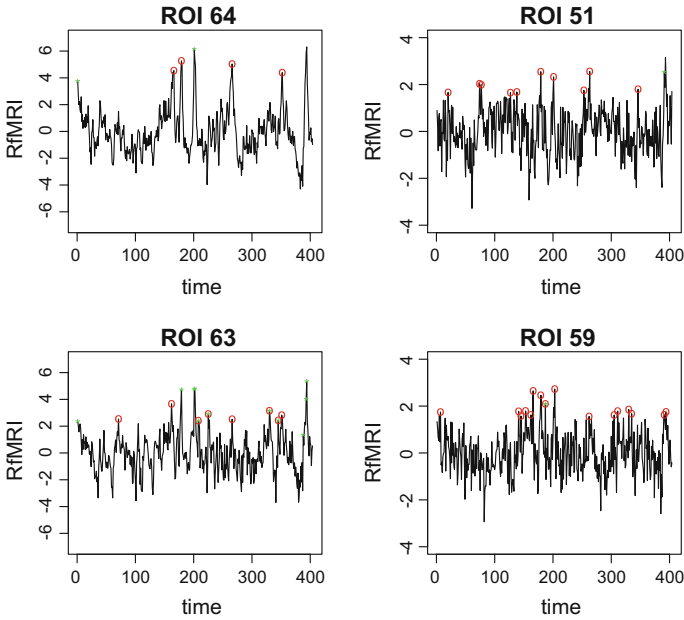


**Fig. 3** Detected spontaneous activations for patient 18 in ROI 64,51,63 and 59. Green stars represent spontaneous activations estimated with robust method, while red dots correspond to the general linear model

vectors in literature, such as Jaccard, Dice, Kulczyńska and Driver and Kroeber (a review is presented in [8]). In this case study, we focus on Dice’s similarity index [11] with expression:

$$\frac{2n_{11}}{2n_{11} + n_{10} + n_{01}}.$$

Given  $\hat{s}_i$  related to two different ROIs,  $n_{11}$  is the total number of activations that occurred at the same time in the two ROIs, while  $n_{10}$  and  $n_{01}$  are activations that occurred in one ROI and not in the other. Dice index ranges from 0 to 1. The results for patient 18 are reported in Fig. 6 while those of patient 22 are reported in Fig. 7. In both figures, we notice that computing the Dice index after the application of the robust method leads to a clearer correlation pattern with respect to computing it after the application of the classical method based on linear model.

Moreover, the highest value of Dice index recorded for patient 18 according to the robust method allows us to detect the following clusters, that are summarized in Fig. 8:

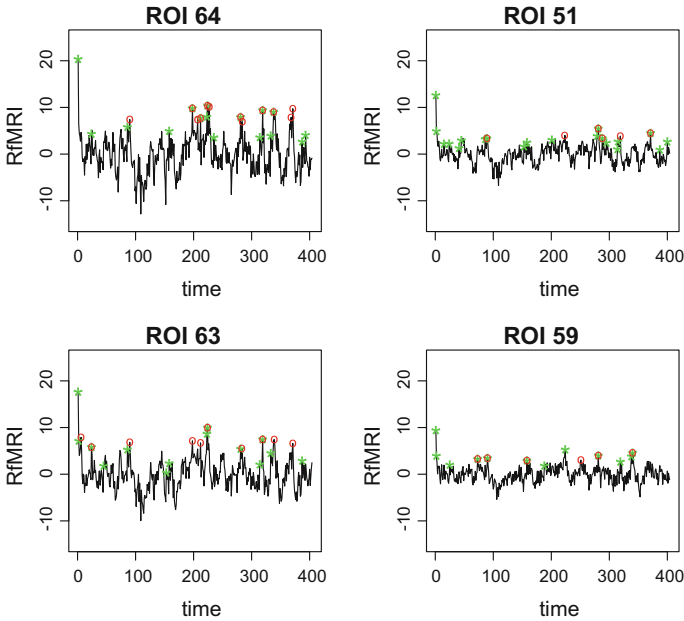


**Fig. 4** Detected spontaneous activations for patient 22 in ROI 64,51,63 and 59. Green stars represent spontaneous activations estimated with robust method, while red dots correspond to the general linear model

- lh-unknown, lh-entorhinal, lh-parahippocampal, lh-transversetemporal (ROIs: 1, 7, 17, 35);
- lh-caudalmiddlefrontal, lh-inferiorparietal, rh-inferiorparietal, rh-postcentral, rh-supramarginal (ROIs: 4, 9, 44, 58, 67);
- lh-rostralmiddlefrontal, lh-superiorfrontal, rh-superiorfrontal (ROIs: 28, 29, 64);
- lh-lateralorbitofrontal, rh-bankssts, rh-corporcallosum, rh-lateralorbitofrontal, rh-medialorbitofrontal (ROIs: 13, 37, 40, 48, 50);
- lh-inferiortemporal, rh-inferiortemporal, rh-middletemporal, rh-precentral (ROIs: 10, 45, 51, 60);
- rh-unknown, rh-entorhinal (ROIs: 36, 42).

Note that ‘lh’ and ‘rh’ stand respectively for the left and right hemispheres. It is interesting to notice that symmetrical ROIs belong to the same groups, such as inferiorparietal, second group, superiorfrontal, third group, lateralorbitofrontal, fourth group and inferiortemporal, fifth group. Moreover, this detection is graphically confirmed by the recorded BOLD, indeed BOLD signals from ROIs of the same group show similar trend (Fig. 8). On the other hand, the highest value of Dice similarity index with the standard approach is 0.55, between lh-lateralorbitofrontal and rh-superiorfrontal.

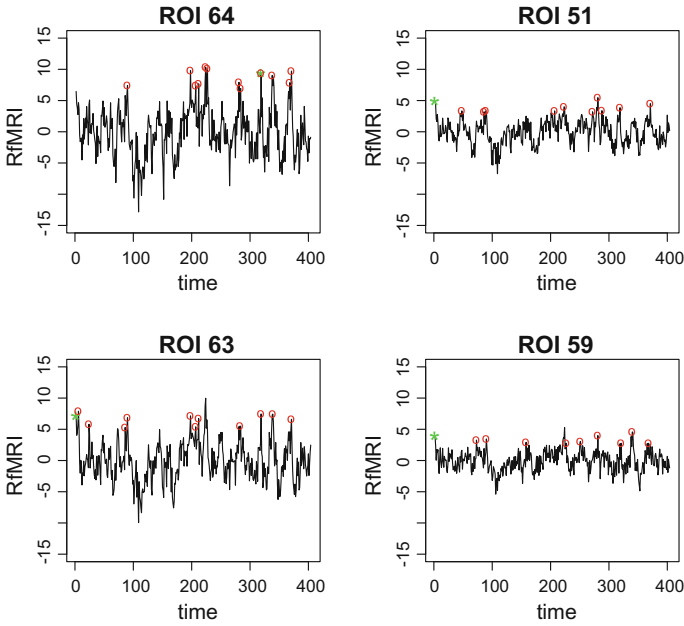


**Fig. 5** Detected spontaneous activations for patient 22 without the first observation in ROI 64,51,63 and 59. Green stars represent spontaneous activations estimated with robust method, while red dots correspond to the general linear model

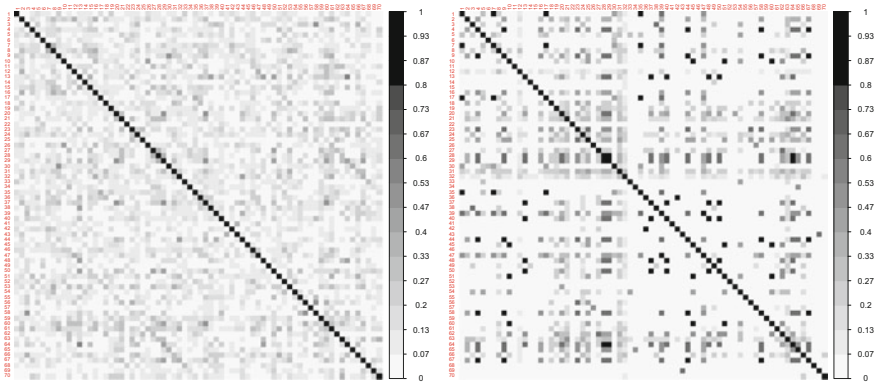


**Fig. 6** Similarity matrix based on Dice distance for patient 18, classical methods (left) robust method (right)

The same analysis can be done on patient 22. For this specific patient, a high peak is recorded in the first time frames as discussed in Sect. 3. If we consider the whole time series, the maximum value of Dice index is recorded for only one group of time series. This group is composed by those RfMRI measures with only one peak at the

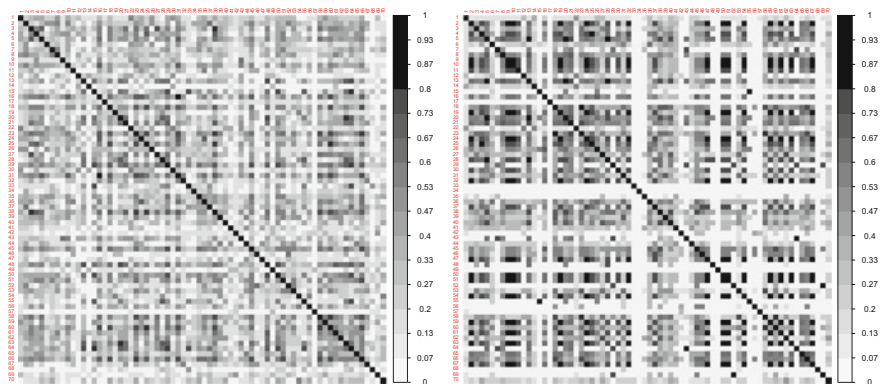


**Fig. 7** Similarity matrix based on Dice distance for patient 22, classical methods (left) robust method (right)

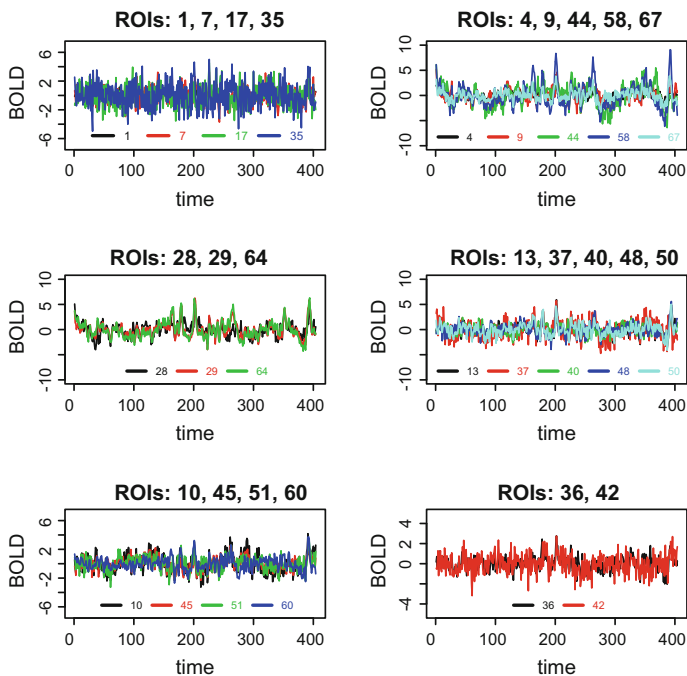


**Fig. 8** BOLD measured in groups with the highest Dice's index for patient 18

beginning. The obtained result is not as informative as the one achieved by detecting peaks on the reduced time series (time series without the first time frames). Focusing on the reduced time series, the highest value of Dice index according to the robust method allows us to detect the following clusters, that are summarized in Fig. 9:

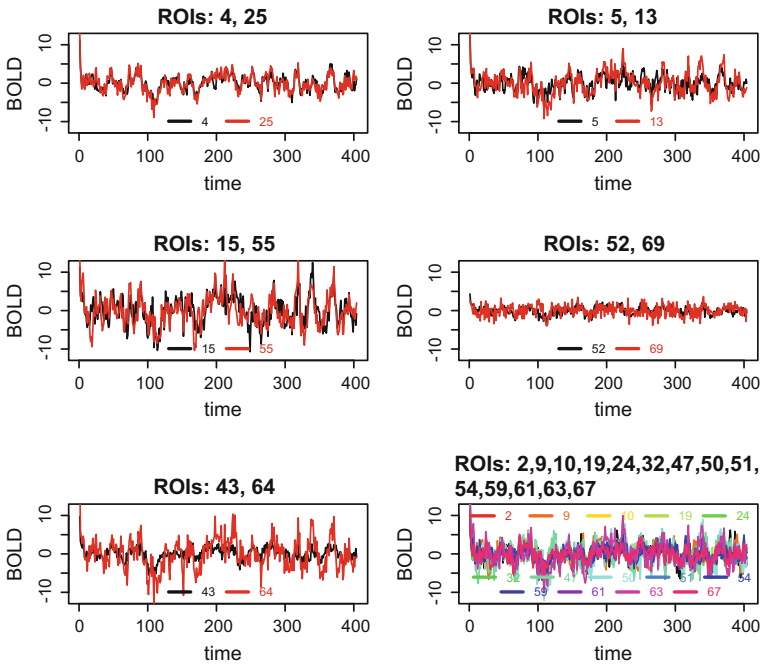


**Fig. 9** BOLD measured in groups with the highest Dice’s index for patient 22

- lh-caudalmiddlefrontal, lh-precentral (ROIs: 4, 25);
- lh-corpuscallosum, lh-lateralorbitofrontal (ROIs: 5, 13);
- lh-medialorbitofrontal, rh-parsorbitalis (ROIs: 15, 55);
- rh-parahippocampal, rh-temporalpole (ROIs: 52, 69);
- rh-fusiform, rh-superiorfrontal (ROIs: 43, 64);
- lh-bankssts, lh-inferiorparietal, lh-inferiortemporal, lh-parsopercularis, lh-posteriorcingulate, lh-supramarginal, rh-lateraloccipital, rh-medialorbitofrontal, rh-middletemporal, rh-parsopercularis, rh-posteriorcingulate, rh-precuneus, rh-rostralmiddlefrontal, rh-supramarginal (ROIs: 2, 9, 10, 19, 24, 32, 47, 50, 51, 54, 59, 61, 63, 67).

The detected pattern is difficult to interpret and requires further investigation.

To conclude, we report in Fig. 10 the estimated HRF in ROIs 64, 51, 63 and 59 for patient 18 and in Fig. 11 the corresponding estimates for patient 22. It is immediate to see that the time-to-peak is similar among all the considered regions, while both the height and the FWHM may be quite different.

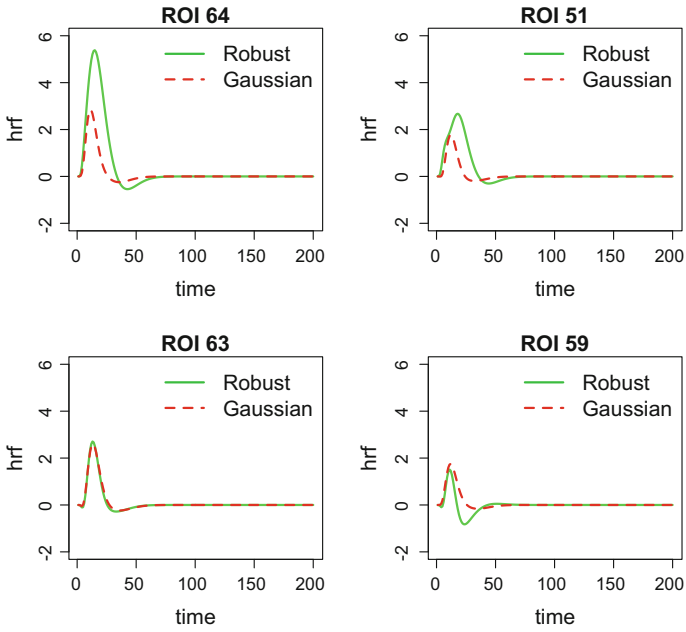


**Fig. 10** Estimated HRF with both methods for patient 18 in ROI 64, 51, 63 and 59

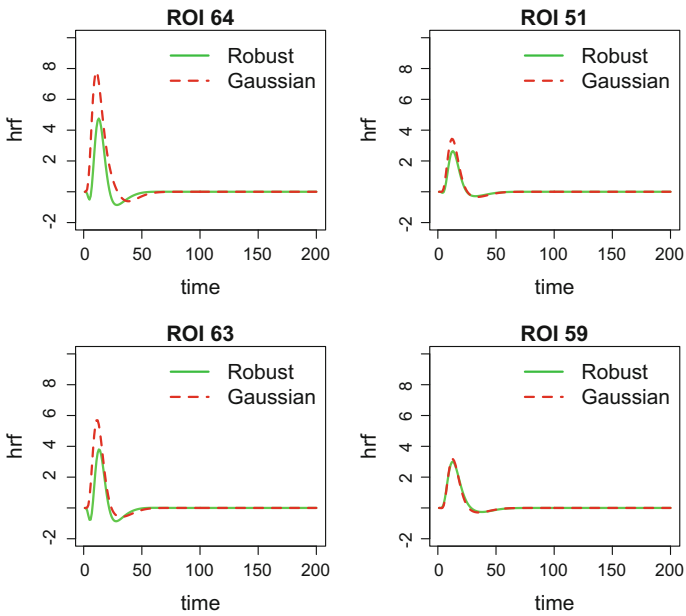


**Fig. 11** Estimated HRF with both methods for patient 22 in ROI 64, 51, 63 and 59



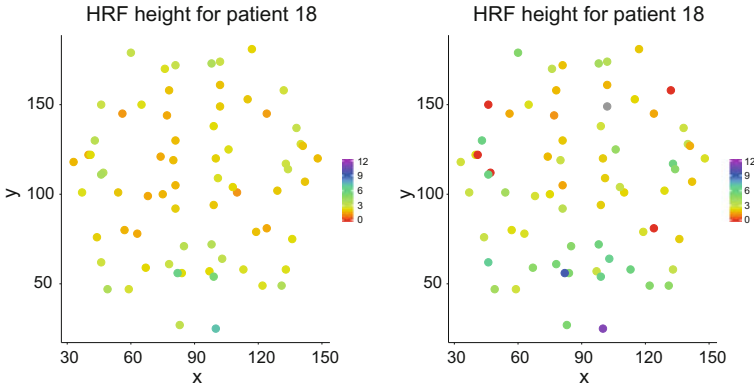


**Fig. 12** Estimated height parameter across ROIs for patient 18 with the classical (left) and robust method (right). This plot shows the estimated height parameter in xy-section of the brain that is obtained by projecting all ROIs centroids in a horizontal plane

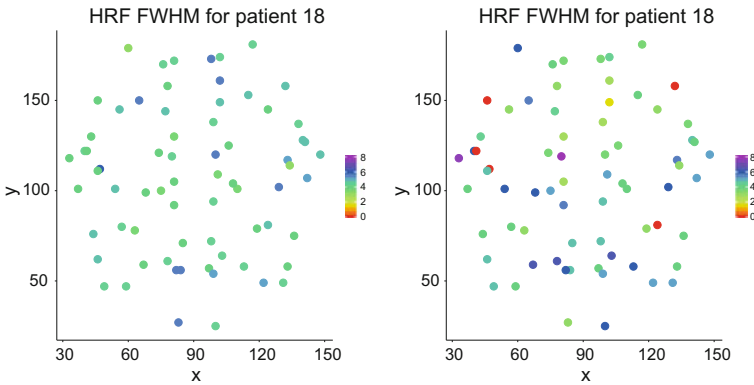


**Fig. 13** Estimated FWHM parameter across ROIs for patient 18 with the classical (left) and robust method (right). This plot shows the estimated FWHM parameter in xy-section of the brain that is obtained by projecting all ROIs centroids in a horizontal plane

In order to have a clearer picture of these differences we plotted the estimated values of these parameters across the regions of interest. The estimated HRF height of patient 18 in a xy-section of brain (horizontal plane of brain) is reported in Fig. 12. The estimated HRF FWHM of patient 18 in a xy-section of brain is reported in Fig. 13. The corresponding pictures for patient 22 are in Figs. 14 and 15. A pattern of height distribution across ROIs seems to be identifiable, but it is still under investigation.

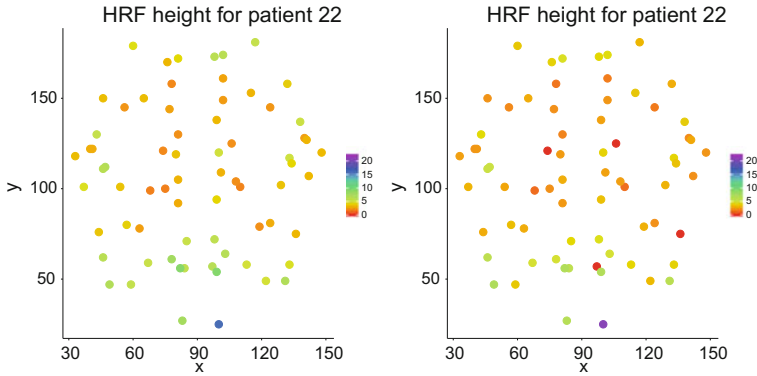


**Fig. 14** Estimated height parameter across ROIs for patient 22 with the classical (left) and robust method (right). This plot shows the estimated height parameter in  $xy$ -section of the brain that is obtained by projecting all ROIs centroids in a horizontal plane

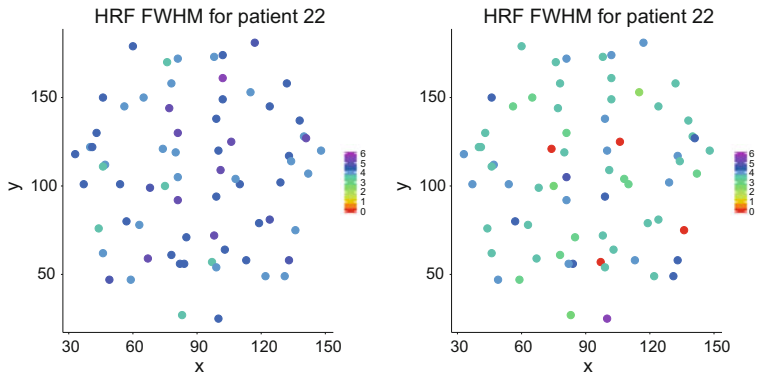


**Fig. 15** Estimated FWHM parameter across ROIs for patient 22 with robust method and a more restrictive cut-off. This plot shows the estimated FWHM parameter in  $xy$ -section of the brain that is obtained by projecting all ROIs centroids in a horizontal plane

## 4 Concluding Remarks and Further Developments

The paper was concerned with the problem of detecting spontaneous activations in resting state fMRI time series and of estimating the hemodynamic response function. Two methods have been considered, one based on a classical, Gaussian, assumption for the data generating process of fMRI data and another based on the assumption that the data may be generated by an heavy tailed distribution. The assumption of a heavy tailed distribution for RfMRI series is supported by the fact that several of the series in the dataset that we have used for our empirical illustrations have shown evidence of extreme values, confirmed by high kurtosis, indicating a violation of the Gaussian assumption. The cut-off threshold used for identifying an observation as

an extreme one, i.e. for detecting a spontaneous event, was rather restrictive, so that fewer spontaneous activations are detected than in the Gaussian case. Methods for determining an optimal threshold may be the object of future investigation.

Future works aim at taking into account the spatial correlation of the data, e.g., by considering a locally anisotropic stationary spatial model, as in the work of Castruccio et al. [6], or by considering spatio-temporal score-driven models, as in [4, 7].

**Acknowledgements** We thank two anonymous referees for their insightful comments and Federico Crescenzi, Michele Peruzzi and Alexios Polymeropoulos for constructive discussions at the Certosa di Pontignano, Bologna and Milano during the initial stages of the current work. We would like to thank Antonio Canale, Daniele Durante, Lucia Paci and Bruno Scarpa for bringing us together and providing us with the challenging dataset analysed in the paper. These data are provided by Greg Kiar and Eric Bridgeford from NeuroData at Johns Hopkins University, who graciously pre-processed the raw DTI and R-fMRI imaging data available at [http://fcon\\_1000.projects.nitrc.org/indi/CoRR/html/nki\\_1.html](http://fcon_1000.projects.nitrc.org/indi/CoRR/html/nki_1.html), using the pipelines ndmg and C-PAC. We would also like to thank all the participants of the StartUp Research event held at the Certosa di Pontignano on June 25-27, 2017, for the stimulating and nice discussions.

## References

1. Aston, J., Kirsch, C.: Evaluating stationarity via change-point alternatives with applications to fMRI data. *Ann. Appl. Statist.* **6**(4), 1906–1948 (2012)
2. Biswal, B., Zerrin Yetkin, F., Haughton, V.M., Hyde, J.S.: Functional connectivity in the motor cortex of resting human brain using echo-planar MRI. *Magn. Reson. Med.* **34**(4), 537–541 (1995)
3. Biswal, B.: Toward discovery science of human brain function. *PNAS* **107**(10), 4734–4739 (2010)
4. Blasques, F., Koopman, S.J., Lucas, A., Schaumburg, J.: Spillover dynamics for systemic risk measurement using spatial financial time series models. *J. Econom.* **195**(2), 211–223 (2016)
5. Bullmore, E., Fadili, J., Breakspear, M., Salvador, R., Suckling, J., Brammer, M.: Wavelets and statistical analysis of functional magnetic resonance images of the human brain. *Statist. Methods Med. Res.* **12**(5), 375–399 (2003)
6. Castruccio, S., Ombao, H., Genton, M. G.: A scalable multi-resolution spatio-temporal model for brain activation and connectivity in fMRI data. *Biometrics* (2018)
7. Catania, L., Billé, A.G.: Dynamic spatial autoregressive models with autoregressive and heteroskedastic disturbances. *J. Appl. Econom.* (2017)
8. Choi, S.S., Cha, S.H., Tappert, C.C.: A survey of binary similarity and distance measures. *J. Syst. Cybern. Inf.* **8**, 43–48 (2010)
9. Creal, D., Koopman, S., Lucas, A.: A dynamic multivariate heavy-tailed model for the time-varying volatility and correlations. *J. Bus. Econom. Statist.* **29**, 552–563 (2011)
10. D’Esposito, M., Deouell, L., Gazzaley, A.: Alterations in the bold fMRI signal with ageing and disease: a challenge for neuro imaging. *Nature Rev. Neurosci.* (4), 863–872 (2003)
11. Dice, L.R.: Measures of the amount of ecologic association between species. *Ecology* **26**(3), 297–302 (1945)
12. Fox, M.D., Raichle, M.E.: Spontaneous fluctuations in brain activity observed with functional magnetic resonance imaging. *Nature Rev. Neurosci.* **8**(9), 700 (2007)
13. Fox, M.D., Snyder, A.Z., Vincent, J.L., Corbetta, M., Van Essen, D.C., Raichle, M.E.: The human brain is intrinsically organized into dynamic, anticorrelated functional networks. *Proc. Natl. Acad. Sci. U. S. A.* **102**(27), 9673–9678 (2005)

14. Friston, K.J., Fletcher, P., Josephs, O., Holmes, A.P., Rugg, M., Turner, R.: Event-related fMRI: characterizing differential responses. *Neuroimage* **7**(1), 30–40 (1998)
15. Friston, K.J., Holmes, A.P., Worsley, K.J., Poline, J.P., Frith, C.D., Frackowiak, R.S.: Statistical parametric maps in functional imaging: a general linear approach. *Huma. Brain Mapp.* **2**(4), 189–210 (1994)
16. Glover, G.H.: Deconvolution of impulse response in event-related BOLD fMRI. *Neuroimage* **9**(4), 416–429 (1999)
17. Handwerker, D.A., Ollinger, J.M., D’Esposito, M.: Variation of BOLD hemodynamic responses across subjects and brain regions and their effects on statistical analyses. *Neuroimage* **21**(4), 1639–1651 (2004)
18. Harvey, A., Luati, A.: Filtering with heavy tails. *J. Am. Statist. Assoc.* **109**(507), 1112–1122 (2014)
19. Harvey, A.C.: *Dynamic Models for Volatility and Heavy Tails: With Applications to Financial and Economic Time Series*. Cambridge University Press (2013)
20. Henson, R., Friston, K.: Convolution models for fMRI. *Statistical parametric mapping: the analysis of functional brain images*, pp. 178–192 (2007)
21. Kruggel, F., von Cramon, D.Y.: Temporal properties of the hemodynamic response in functional MRI. *Hum. Brain Mapp.* **8**(4), 259–271 (1999)
22. Lange, N., Zeger, S.L.: Non-linear fourier time series analysis for human brain mapping by functional magnetic resonance imaging. *J. Royal Statist. Soc. Ser. C (Appl. Statist.)* **46**(1), 1–29 (1997)
23. Lindquist, M.A.: The statistical analysis of fMRI data. *Statist. Sci.* **23**(4), 439–464 (2008)
24. Lund, T.E.: Non-white noise in fMRI: Does modelling have an impact? *Neuroimage* **29**(4), 1639–1651 (2006)
25. Poldrack, R.A., Mumford, J.A., Nichols, T.E.: *Handbook of Functional MRI data Analysis*. Cambridge University Press (2011)
26. Woolrich, M.W., Ripley, B.D., Brady, M., Smith, S.M.: Temporal autocorrelation in univariate linear modeling of fMRI data. *Neuroimage* **14**(6), 1370–1386 (2001)
27. Worsley, K.J., Liao, C., Aston, J., Petre, V., Duncan, G., Morales, F., Evans, A.: A general statistical analysis for fMRI data. *Neuroimage* **15**(1), 1–15 (2002)
28. Worsley, K.: Detecting activation in fMRI data. *Statist. Methods Med. Res.* **12**(5), 401–418 (2003)
29. Wu, G.R., Liao, W., Stramaglia, S., Ding, J.R., Chen, H., Marinazzo, D.: A blind deconvolution approach to recover effective connectivity brain networks from resting state fMRI data. *Med. Image Anal.* **17**(3), 365–374 (2013)